Arabian Journal of Chemistry (2022) **15**, 104309

King Saud University

Arabian Journal of Chemistry

www.ksu.edu.sa
www.sciencedirect.com

ORIGINAL ARTICLE

Pencil graphite supported nano zero-valent iron for removal of levofloxacin from aqueous solution: Effects of pH, kinetic and biological activity

Abdulla S. Idrees [a], Saleh M. Sulaiman [a,*,1], Mohammed H. Al-Jabari [a,*,1], Mazen K. Nazal [b], Asem M. Mubarak [a], Leena N. Al-Rimawi [a]

[a] *Department of Chemistry, Faculty of Science, Birzeit University, Birzeit, P.O. Box 14, Ramallah, West Bank, Palestine,State of*
[b] *Center for Environment and Water, Research Institute, King Fahd University of Petroleum and Minerals, Dhahran 31261, Saudi Arabia*

Received 8 July 2022; accepted 26 September 2022
Available online 1 October 2022

KEYWORDS

Adsorption;
Antibacterial agent;
Fluoroquinolone;
Fe^0;
Composite

Abstract A highly efficient, and potentially recyclable antibacterial composite was prepared in an efficient simple process. Antimicrobial levofloxacin (LEV) was used to functionalize the surface of nano zero-valent iron (Fe^0) supported by pencil graphite (PG). The surface morphology, elemental composition, particle size, and removal efficiency of the PG-Fe^0 composite were confirmed by UV, FTIR, EDX, SEM, TEM, and XRD techniques. The potential influence of pH, adsorbate concentration, contact time, and temperature on the removal efficiency of LEV by the magnetic composite (PG-Fe^0) from an aqueous solution was investigated. The well-known established models were used to examine the adsorption isotherms, and the results showed that the kinetic adsorption data fit well with the pseudo-second-order model, with the highest removal efficiency achieved from pH 5–7 (85%). The maximum adsorption capacity (q_{max}) on the surface of Fe^0-PG for LEV was obtained using the Langmuir isotherm at pH 6.5 (66.3 mg/g) and pH 8 (11.4 mg/g). All adsorption thermodynamic parameters at pH 6.5 suggested a chemisorption endothermic natural process ΔH^o(44.4 kJ/mol), and the negative value of free Gibbs energy indicated a spontaneous process at an ambient temperature. Furthermore, the removal efficiency of the PG-Fe^0 composite was better than that of the Fenton-like catalyst performance for both Fe^0 and PG-Fe^0. Reusability and antibacterial activity of adsorbed LEV on the surface of PG-Fe^0 were investigated against various types of gram-positive bacteria; (E. faecalis, S. epidermidis, and S. aureus) and gram-negative;

* Corresponding authors.
E-mail addresses: ssuliaman@birzeit.edu (S.M. Sulaiman), maljabari@birzeit.edu (M.H. Al-Jabari).
[1] The second and third authors have identical contributions to this paper.

Peer review under responsibility of King Saud University.

Production and hosting by Elsevier

https://doi.org/10.1016/j.arabjc.2022.104309

(E. coli, K. pneumonia, and P. Mirabilia) via agar well diffusion method. Finally, the magnetic feature of the PG-Fe^0-LEV composite has numerous potential for recovery and reuse.

1. Introduction

Antibiotics in the environment have recently received a lot of attention due to the cumulative contribution and release of antibiotic residue into the environment, which deteriorates ecosystem health and increases antibiotic resistance for bacteria and genes (Kemper, 2008; Ashfaq et al., 2016).

The fluoroquinolone (FQ) antibiotic has a high level of tolerance and potency to treat infectious diseases (Park et al., 2002; Samuelsen, 2006). According to the literature; FQs are the most frequently identified antibiotic group, followed by tetracyclines, sulfonamides, and macrolides (Schlüsener and Bester, 2006; Ji et al., 2013). However, these drugs are poorly absorbed and digested in the human/animal body and are mostly excreted in their active pharmacological form in the urine/feces (Verlicchi et al., 2010). The continuous influx of FQs into aqueous environments even at low concentrations endangers water safety and aquatic ecology, and according to EPA guidelines, the toxicity value of LEV concentration level for discharge to water or environment ranges from 1.1 to 23 mg/L (Luo et al., 2014; Graham et al., 2006).

LEV is a fluoroquinolone antibiotic ($C_{18}H_{20}FN_3O_4$, 361.368 g/mol is an S-(-) optical isomer of ofloxacin) with antibacterial activity against both gram-positive and gram-negative bacteria (Anderson and Perry, 2008). At various pH values, the cationic, anionic, neutral, and zwitterionic activity of chemical LEV structures are demonstrated (Fig. 1) (Anderson and Perry, 2008; Qin et al., 2014). LEV is usually present in its cationic form at low pH, but it is mostly present in its anionic form at pH > 7 and is primarily present in zwitterionic and neutral forms at pH values ranging from 5.0 to 7.0 (Qin et al., 2014).

The persistence of chemical pollutants has posed a challenge to the aquatic environment, prompting the development of numerous approaches and water treatment technologies, including adsorption (Wang et al., 2022a, 2022b), photocatalysis (Liu et al., 2022; Zhu et al., 2022), advanced oxidation (The Fenton-like process has been extensively investigated for its potential in water purification and soil remediation) (Yang et al., 2022a, 2022b), and microwave catalysis (Wang et al., 2020). Adsorption has advantages over other methods because it is environmentally friendly, has a simple design (technologically simple and applicable to many treatment patterns), and requires low investment in terms of both land and cost (materials locally available). A variety of adsorbents have been used to remove LEV from the contaminated water, including Fe_3O_4, magnetic mesoporous carbon composite, magnetic graphene oxide-grafted cellulose nanocrystal molecularly imprinted polymers, and so on (Wang et al., 2017; Al-Jabari et al., 2019). Even though some of these adsorbents have been demonstrated to have high LEV removal efficiency, the majority of the reported studies do not investigate the impact of pH on the removal efficiency or potential reusability of the LEV after adsorption.

Zero valent iron nano-particles (Fe^0 NPs) have recently received a lot of attention in adsorption technology due to their high specific surface area, more active intrinsic surface sites, and greater ability to chemically reduce resistant compounds (Li et al., 2008; Qian et al., 2019; Yu et al., 2020). In the environment, Fe^0 NPs were widely used for the removal of organic and inorganic contaminants and as a catalyst in the degradation of organic compounds (Wang et al., 2022a, 2022b; Yang et al., 2022a, 2022b). However, Fe^0 NPs tend to react and agglomerate, resulting in a significant reduction in their reactivity (Ponder et al., 2000). As a result, many particle-stabilizing strategies for efficient Fe^0 NPs diffusion and sorption have been investigated, including the use of activated carbon, clay, mesoporous silica, magnetite, biochar, and hematite as supporting materials to improve the dispersity and stability of Fe^0 NPs in aqueous media (Chen et al., 2011; Sulaiman and Shahwan, 2017; Al-Jabari et al., 2019; Shen et al., 2020; Sulaiman and Al-Jabari, 2021; Gong et al., 2022).

Pencil-graphite (PG) is a hybrid material composed of graphite (65 %), clay (30 %), and a binder substance (such as wax, resin, or high polymer) (Agrawal, 2008). The PG is denoted by the European letters H (hard) and B (black), with numbers ranging from 9H (hardest) to 8B (blackest or softest), the B-type is softer and contains more graphite, while the H-type is harder and contains more clay, and the HB-type contains equal parts graphite and clay (Agrawal, 2008; Taylor, 2013). PG has a large surface area and is easily surface functionalized forming specific binding sites, higher adsorption capacity, and low cost. Furthermore, PG is now recognized as a pencil graphite electrode (working electrodes), and the modified PG electrodes have recently been used in potentiometric techniques to detect organic and inorganic substances, these advantages have proposed the PG as a supporting material for Fe^0 NPs (Tavares and Barbeira, 2008; David et al., 2017; Kolahi-Ahari et al., 2020).

In this study, the adsorption properties, possible removal, reusability, and mechanism of LEV on the surface of the PG-Fe^0 composite were investigated. The synthesized materials were characterized using established material characterization techniques. The Fenton-like process and the effect of variable parameters on removal efficiency (pH, adsorbate concentration, contact time, and temperature) were investigated. The adsorption isotherm models of Langmuir and Freundlich were used to investigate the mechanism of LEV adsorption onto the surface of the PG-Fe^0 composite at various pH values. The kinetics, adsorption isotherms, and thermodynamic factors were studied to better understand the mechanism of adsorption. Finally, the biological activity of PG-Fe^0-LEV was evaluated using the agar-well diffusion method.

2. Experimental

2.1. Chemicals

Ferric chloride hexahydrate ($FeCl_3{\cdot}6H_2O$, ≥ 99 %), Absolute ethanol (C_2H_5OH, ≥ 99 %), Sodium borohydride ($NaBH_4$, ≥ 97 %), Pencil lead graphite (HB, 0.5 mm), and Levofloxacin ($C_{18}H_{20}FN_3O_4$, ≥ 99 %), Milli-Q water (Resistivity = 18.2 MΩ.cm), Nitrogen gas N_2 ≥ 99 %, Hydrochloric acid (0.1 M HCl), Sodium hydroxide (0.1 M NaOH), and sodium chloride (0.1 M NaCl). All bacterial strains (Escherichia coli, Staphylococcus aureus, Proteus mirabilis, Klebsiella pneumonia, Staphylococcus epidermidis, and Enterococcus faecalis) were donated by the Department of Biology and Biochemistry at Birzeit University.

2.2. Synthesis of pencil graphite supported zero-valent iron nanoparticles

Pencil graphite supported nano zero-valent iron (PG-Fe^0) was synthesized using the liquid-phase reduction method (Chen et al., 2011).

$$4Fe^{3+} + 3BH_4^- + 9H_2O \rightarrow 4Fe^0 + 3H_2BO^{3-} + 12H^+ + H_2\uparrow(g).$$

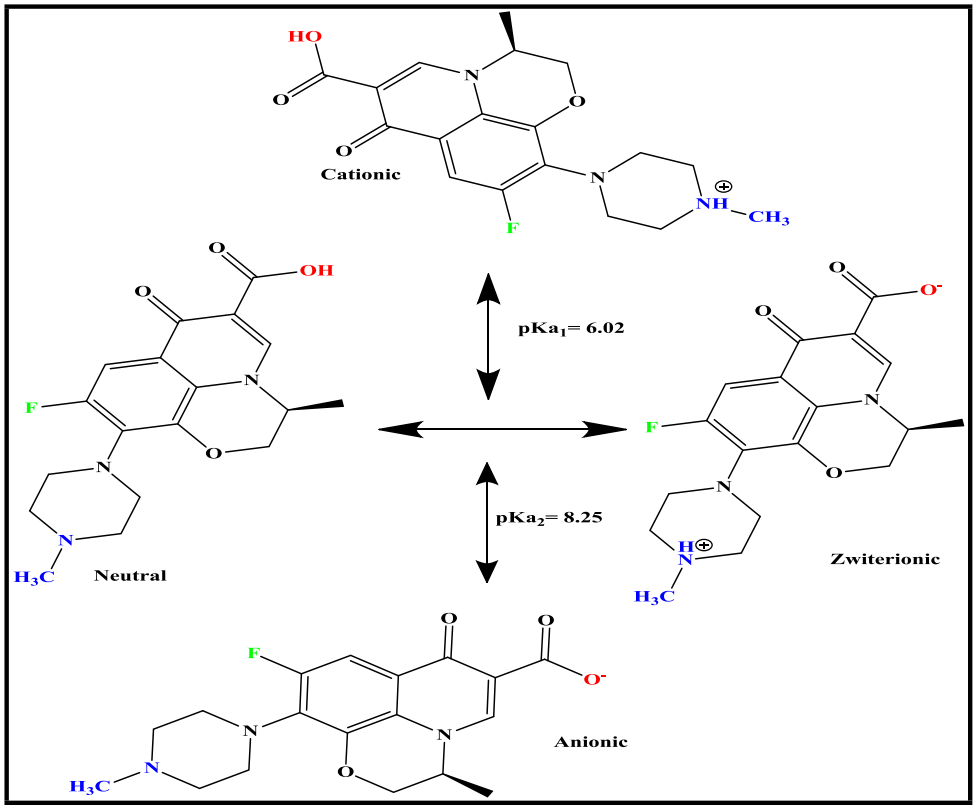

Fig. 1 The pH-dependent chemical structures of the levofloxacin drug (Qin et al., 2014).

The previously established method was used to synthesize the PG-Fe^0 composite (Al-Rimawi et al., 2022). The preparation consisted of PG-Fe^0 with an iron/pencil graphite mass ratio of (1:1). 4.84 g of Ferric chloride hexahydrate ($FeCl_3 \cdot 6H_2O$) was dissolved in 100 mL of miscible liquids (Milli-Q water and absolute ethanol at a volume ratio of 1:4 v/v), followed by 4.84 g of milled pencil graphite were added to the solution. The mixture was stirred vigorously under a nitrogen atmosphere for 15 min, then 100 mL 0.47 M $NaBH_4$ solution was added dropwise to the mixture at a rate of 1–2 drops per second. After all of the $NaBH_4$ solution had been added, the mixture was continuously stirred for a further 20 min under a nitrogen atmosphere to completely deplete $NaBH_4$ and $FeCl_3 \cdot 6H_2O$ The composite was thoroughly washed with water and ethanol before being collected and dried under vacuum at room temperature. The composite was then sealed in a bottle for future use, and the amount of Fe^0 NPs on the surface of PG was estimated to be 160 mg/g.

2.3. Characterization techniques

The diffraction patterns of PG-Fe^0 composite were obtained using mini-XRD (Rigaku Ultima, Tokyo, Japan) with a CuK α source and 2θ angles in the range from 0−65° at a slow scan rate of 2θ/ min. A UV–vis Spectrophotometer (Hp 8453, Agilent, USA) was used to measure solution absorption over a wavelength range of 190–1100 nm. Fourier transform infrared (FTIR) spectra were recorded in the range of 4000–230 cm^{-1} using (a Bruker TENSOR II Spectrometer), and sample pellets were prepared by combining the analyte with KBr in a corresponding ratio of 1:200 (w/w). The composite images were captured using the JOEL-2100F field emission transmission electron microscope (FE-TEM) and scanning electron microscopy (SEM) coupled with energy dispersive X-rays (SEM-EDX) (Jeol 6700LV).

3. Adsorption experiments

A stock LEV solution (100 mg/L) was prepared in deionized water to avoid any interference that might affect the adsorption of LEV molecules on the PG-Fe^0 surface, and serial dilutions were obtained to construct a calibration curve in the concentration range of 2.5–40 mg/L (**Fig. S1**). The UV–vis Spectrum for each solution was measured at a maximum wavelength of 289 nm. The analyses for each sample were repeated three times, and the mean values were considered with a maximum error of less than 2.0 %.

3.1. Effect of pH

At different initial pH values (3.0, 5.0, 6.5, 8.0 and 10.0) 100 mL of 20 mg/L LEV solutions were prepared. The solutions were adjusted to the appropriate pH using 0.1 M NaOH and 0.1 M HCl solutions. Each solution received 0.5 g of PG-Fe^0 composite before being shaken in a water bath shaker for 3 h at a constant temperature of 298 K and 125 rpm. When equilibrium was established, the concentration of LEV was determined by taking a 5 mL aliquot from each solution and

measuring the absorption of LEV with a UV–visible spectrophotometer. Then, the concentration of LEV in each solution was calculated.

3.2. Effect of adsorbent dose

To evaluate the optimal amount of adsorbent dose required for LEV adsorption, a different dose of the PG-Fe^0 composite (0.1, 0.5, 1.0, and 1.5 g) was applied to 100 mL of 25 mg/L LEV solution. The mixtures were shaken at 125 rpm for 3 h at 298 K and pH 6.5. After equilibrium was established, each solution was filtered through a 0.45 μm filter, and the removal efficiency in each solution was calculated.

3.3. Effect of contact time and adsorbate concentration

The kinetic study was carried out at two different pH values (pH = 6.5 and pH = 8). For that, concentrations of LEV solutions were prepared (10, 20, 25, 30, and 35 mg/L) at appropriate pH, followed by the addition of 0.5 g of adsorbent material. After that, all solutions were shaken for 3 h at 125 rpm and 298 K. All samples were analyzed at various time intervals (5, 10, 15, 20, 30, 40, 80, and 320 min). At the end of the contact time, the adsorbent composite was collected by an external magnetic field and the aliquot was filtered through 0.45 μm membrane filters. The LEV absorption in the supernatant solution was analyzed before and after the adsorption process, and the concentration of LEV was calculated using a calibration curve (**Fig.S1**). The removal efficiency of the adsorbent was determined according to Eq. (1),

$$\%Removal = \frac{C_0 - C_e}{C_o} * 100\% \quad (1)$$

3.4. Effect of temperature

The removal efficiency of LEV was investigated as a function of temperature for 100 mL of 20 mg/L LEV solution at 278, 288, 298, and 308 K. At each temperature and pH 6.5, 0.5 g of PG-Fe^0 composite was added to the corresponding LEV solution. The solutions were shaken for 3 h in a thermostatic shaker at 125 rpm. Samples from each solution were collected at various time intervals (5, 10, 15, 20, 30, 40, 80, and 320 min), then the collected samples were filtered through a 0.45 μm filter, and the absorbance of the aliquot from each sample was measured to determine the LEV concentrations.

3.5. Fenton catalyst

LEV removal was also investigated using a Fenton-like reaction, which involved exposing 0.5 g of PG-Fe^0 composite (equivalent to 80 mg Fe^0) to 90.0 mL of 10 mg/L LEV solution and 10 mL of freshly prepared H_2O_2. The solution was then kept in a thermostatic shaking water bath at 298 K for two hours before the absorbance of the separated LEV solution was measured.

3.6. Antimicrobial activity

The antimicrobial activity of PG-Fe^0-LEV was investigated using the well-agar diffusion method. Gram-positive (E. faecalis, S. epidermidis, and S. aureus) and gram-negative (E. coli, K. pneumonia, and P. mirabilis) bacteria were used. The PG-Fe^0-LEV composite was made by combining 0.5 g of PG-Fe^0 composite with 100 mL of 25 mg/L LEV solution and shaking it continuously at 125 rpm. After 300 min of adsorption, the composite was collected and dried using an external magnetic field, and a UV–vis spectrophotometric analysis method was used to determine the concentration of adsorbed LEV. The optimal concentrations of PG-Fe^0-LEV, PG-Fe^0 composite, and LEV were calculated, and Milli-Q water was used as a negative control. The bacterial strains were evenly distributed across the Mueller-Hinton agar plate. After piercing a 6 mm hole with a sterile head, 50 μL of each antimicrobial agent was injected into the wells of agar, and for 24 h the plates were incubated at 310 K. Finally, the samples were duplicated, and the average diameter of the final inhibition zone was measured.

4. Results and discussion

4.1. Characterization of PG-Fe^0 composite

To characterize the surface morphology of synthesized materials, SEM, TEM, EDS, XRD, and FTIR techniques were used. TEM and SEM images for aggregated chains of Fe^0 NPs with an average diameter of about 60 nm are shown in Fig. 2 (a, b). Aggregation of Fe^0 NPs reduces the surface area and limits the dispersion of Fe^0 NPs in the solution causing a drop in pollutant removal efficiency. SEM images of milled pencil graphite that appeared as bonded sheets and flakes are shown in Fig. 2 (c), and SEM images of the PG-Fe^0 composite are shown in Fig. 2 (d). The image depicts Fe^0 NPs adhering and dispersing on the PG surface. Furthermore, the Fe^0 NPs adhere tightly to the PG surface, and the composite is strongly attracted to an external magnetic field. The aggregation of the Fe^0 NPs was reduced as soon as the Fe^0 NPs spread across the PG surface. The elemental analysis of PG, Fe^0, and PG-Fe^0 composite was evaluated using energy-dispersive X-ray spectroscopy (EDS). The EDS spectrum of the PG-Fe^0 composite is depicted in (**Fig.S2**), and the analysis confirmed the presence of the main elements in the composite.

The XRD characterization technique was used to determine the crystalline morphology of the Fe^0 and PG-Fe^0 composite; the diffraction pattern of the Fe^0, as shown in Fig. 3 (a), demonstrated the presence of crystalline zero-valent iron in the sample with a basic reflection peak at $2\theta = 44.9°$ (110 reflectance), which illustrates the distribution of small size particles for a metallic iron crystal (Fe^0), the reflectance peak of iron oxide was very weak, implying that Fe^0 is the main component of iron nanoparticle materials. While Graphite showed characteristic peaks at $2\theta = 26.7°$ and $2\theta = 55°$, as shown in Fig. 3 (b) (Sun et al., 2006). While Fig. 3 (c) depicts the XRD spectrum diffraction angles of the PG-Fe^0 at (2θ) 26.7°, 44.9°, and 55°, respectively. These reflections from (002), (110), and (004), are assigned to the Fe^0 and PG and demonstrate the presence of Fe^0 on the PG surface (Yuan et al., 2008; Skrzypczynska et al., 2018; Xu et al., 2018). After LEV adsorption via Fe^0 loaded on the PG surface, no change in the position of the distinctive peak for PG (002) was observed, implying that no phase transformation occurred. Whereas the distinctive peak of Fe^0 (110) was shifted to the right,

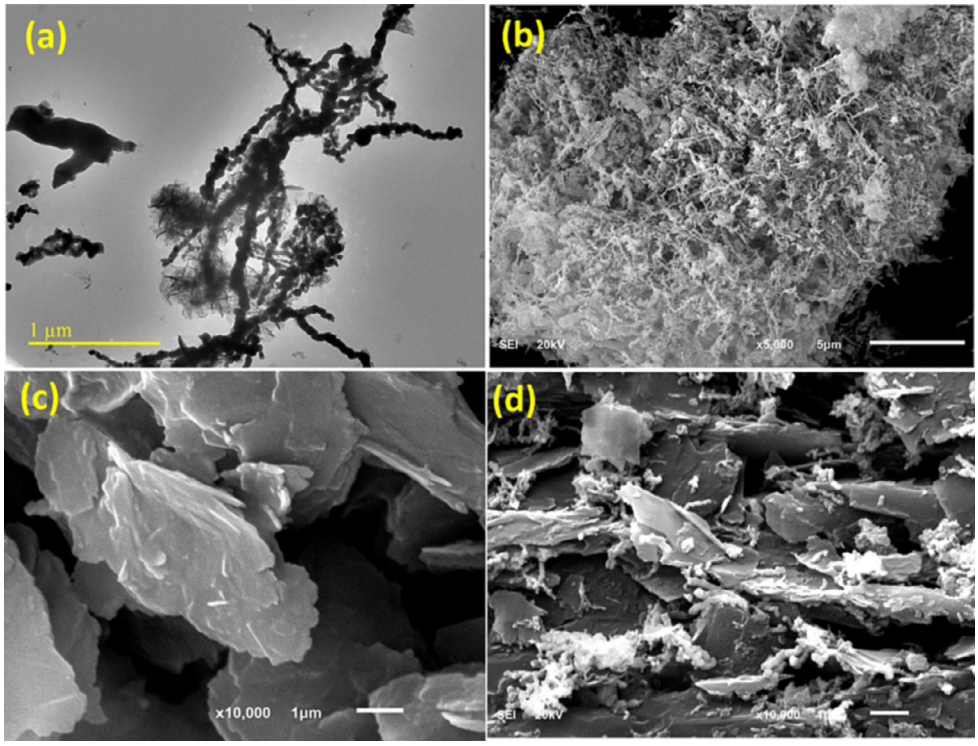

Fig. 2 (a) and (b) are TEM and SEM images of Fe^0 NPs respectively. (c) and (d) are SEM images of PG and PG-Fe^0 composite, respectively.

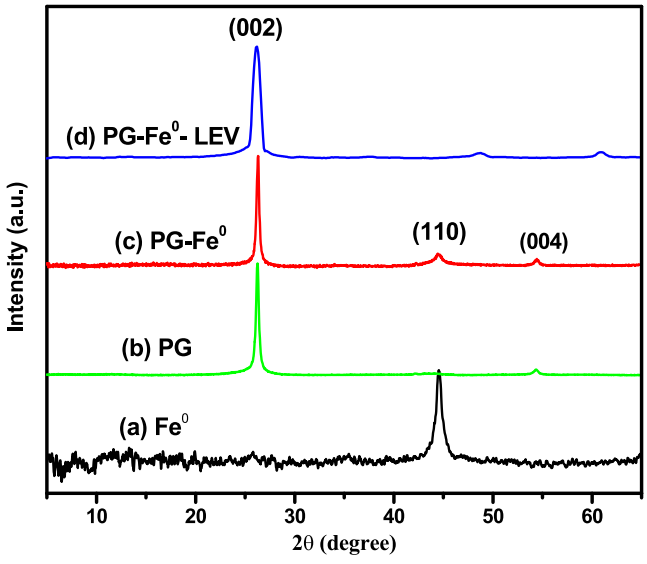

Fig. 3 The XRD patterns of (a) Fe^0 NPs, (b) PG, (c) PG-Fe^0 composite, and (d) Fe^0-PG-LEV.

indicating LEV attachment to the surface of Fe^0 NPs (Fig. 3 d) (Ben Arfi et al., 2017).

The coordination mode between ligand (LEV) and metal (Fe^0) was identified using FTIR spectroscopy after LEV adsorption (Fig. 4). For this purpose, the sodium levofloxacin (Na_{levo}), PG-Fe^0, and PG-Fe^0-LEV FTIR spectra were obtained in the range of 4000–230 cm^{-1}. The probable modes are monodentate ($\Delta\nu(COO^-)_{complex} \gg \Delta\nu(COO^-)_{Na}$), bidentate chelating ($\Delta\nu(COO^-)_{complex} \ll \Delta\nu(COO^-)_{Na}$), or bidentate bridging ($\Delta\nu(COO^-)_{complex} \approx \Delta\nu(COO^-)_{Na}$). The Na_{levo} spectrum in Fig. 4 (a) showed the absorption peak for the pyridone $\nu(C{=}O)_p$ at 1616 cm^{-1} and the peak of the carboxylate stretch $\nu(C{=}O)_{carb}$ at 1721 cm^{-1}. In PG-Fe-LEV composite spectrum, the peak of the carboxylic group $\nu(C{=}O)_{carb}$ has disappeared upon binding and the two characteristic peaks asymmetric $\nu(COO^-$, 1586 $cm^{-1})_{asym}$ and symmetric $\nu(COO^-$,1392 $cm^{-1})_{sym}$ stretching vibrations was shifted to 1620 cm^{-1} and 1395 cm^{-1}, respectively. The difference between the two peaks $\Delta\nu(COO^-)$ = 225 cm^{-1} which is greater than in Na_{levo} $\Delta\nu(COO^-)$ = 194 cm^{-1} indicating the monodentate coordination mode of the carboxylate group. Similarly, the carbonyl pyridone $\nu(C{=}O)_p$ is shifted from 1616 cm^{-1} to 1580 cm^{-1} upon bonding. The overall changes indicate that levofloxacin was bonded to the PG-Fe^0 composite through the pyridone oxygen atom and one of the oxygen atoms from the carboxylate group as shown in Fig. 5 (Turel, 2002; Uivarosi, 2013; Mimouni et al., 2018). Generally, the ν(M−N) and ν(M−O) for metal complexes bands appear in the range of (230–700) cm^{-1} (Alabdali and Ibrahim, 2014). The broad split peak between 3500 and 3100 cm^{-1} is assigned to the O—H and N—H stretching of H_2O molecules and piperazinyl moiety, respectively (Qassim, 2015).

4.2. The effect of pH and adsorbent dose on LEV removal

As shown in Fig. 6 (a), different composite doses of PG-Fe^0 ranging from 0.1 to 1.5 g were investigated for LEV removal efficiency. When an adsorbent dose is increased, the removal efficiency increases from 30 % to 78 % due to the availability

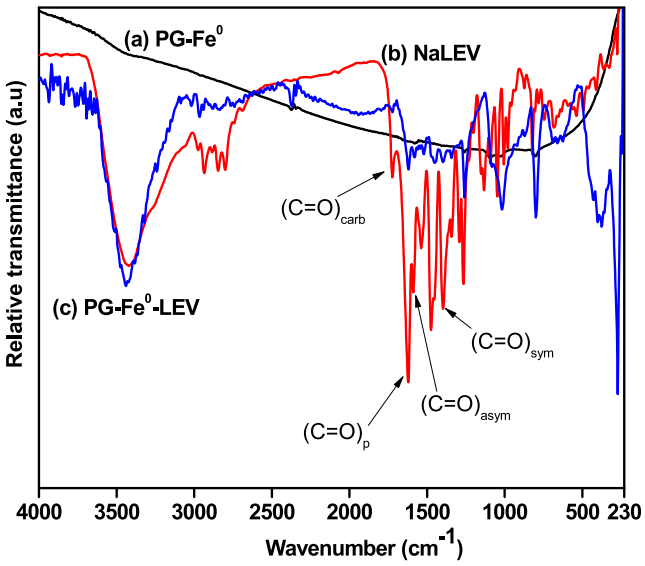

Fig. 4 FTIR spectra of (a) NaLEV, (b) PG-Fe^0 composite (c) PG-Fe^0-LEV composite.

of the free locations and the unsaturation adsorption sites (i.e., more surface area). The adsorption efficiency also decreased from 78 % to 50 % at 1.5 g, which could be explained by the ability of particles to aggregate by increasing their amount, resulting in a decrease of free adsorbent sites. However, an increase in performance occurs only after a certain amount of adsorbent dose is added, after that, performance becomes constant.

The chemical structure of LEV is pH-dependent, and the pH value is an important parameter that influences LEV adsorption using the PG-Fe^0 composite. Fig. 6 (b) depicts the effect of pH on the adsorption of LEV in an aqueous solution with a composite adsorbent. As shown, the removal of LEV increases as the pH rises from 3 to 5, and LEV molecules appear in the cationic form LEV^+. The cationic form of LEV^+ gradually decreases as the pH rises, and LEV molecules are converted to the Zwitterionic form. The maximum adsorption of LEV onto PG-Fe^0 composite occurs when the chemical structure is neutral/zwitterion (pH 5–7). As the pH of the LEV solution increased from 7 to alkaline, a gradual decrease in LEV removal was observed, indicating that LEV molecules have the anionic form (LEV^-). The aspect of maximum exclusion of LEV molecules at pH > 7 or at pH > 7 can be attributed to ion exchange. Moreover, as the pH increases or decreases, the removal efficiency decreases due to electrostatic repulsion between similar charges. Furthermore, as shown in Fig. 6 (c), the removal efficiency of LEV by composite in different initial concentrations is more efficient at pH 6.5 than at pH 8. At both pH values, the maximum removal efficiency was at 10 mg/L of LEV and decreased as the initial concentration increased; further kinetic and thermodynamic analysis will be performed in the following sections. On the other hand, the performance of the milled PG is insufficient to remove LEV from aqueous solutions for all concentrations at both pH values.

4.3. LEV removal kinetic

Kinetic experiments were carried out at two different pH values (pH = 6 and pH = 8) to investigate the adsorption rate as well as the kinetic mechanism of the adsorption process. The amount of LEV adsorbed onto the PG-Fe^0 composite surface was calculated using the mass balance equation Eq.(2) (Thilagan et al., 2013).

$$Q = (C_0 - Ce)\frac{V}{m} \tag{2}$$

Where Q is the adsorbent's concentration of LEV removal (mg/g). C_0 represents the initial concentration of LEV (mg/L). C_e indicates the concentration of LEV in solution at a given time. V indicates the volume of the solution (L), and m indicates the mass of the adsorbent (mg). Lagergren pseudo-first-order and pseudo-second-order models were used to test the experimental data of LEV adsorption by PG-Fe^0 composite (Vijayakumar et al., 2012; Ho, 2014).

The linear Lagergren pseudo-first-order model is represented as Eq.(3) (Simonin, 2016; Fu et al., 2021):

$$\ln(q_e - q_t) = \ln q_e - k_1 t \tag{3}$$

Where q_e and q_t are the amounts of LEV that are adsorbed by the adsorbent in equilibrium and at any time (mg/g), respectively. k_1 is the first-order rate constant (min^{-1}) and t is the

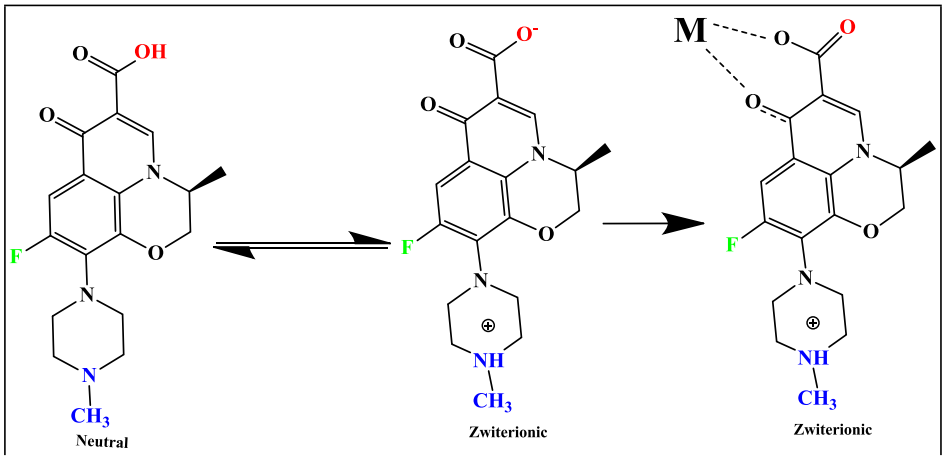

Fig. 5 Schematic represents the suggested adsorption mechanism of LEV onto the surface of the PG-Fe^0 composite (M), pH = 6.5.

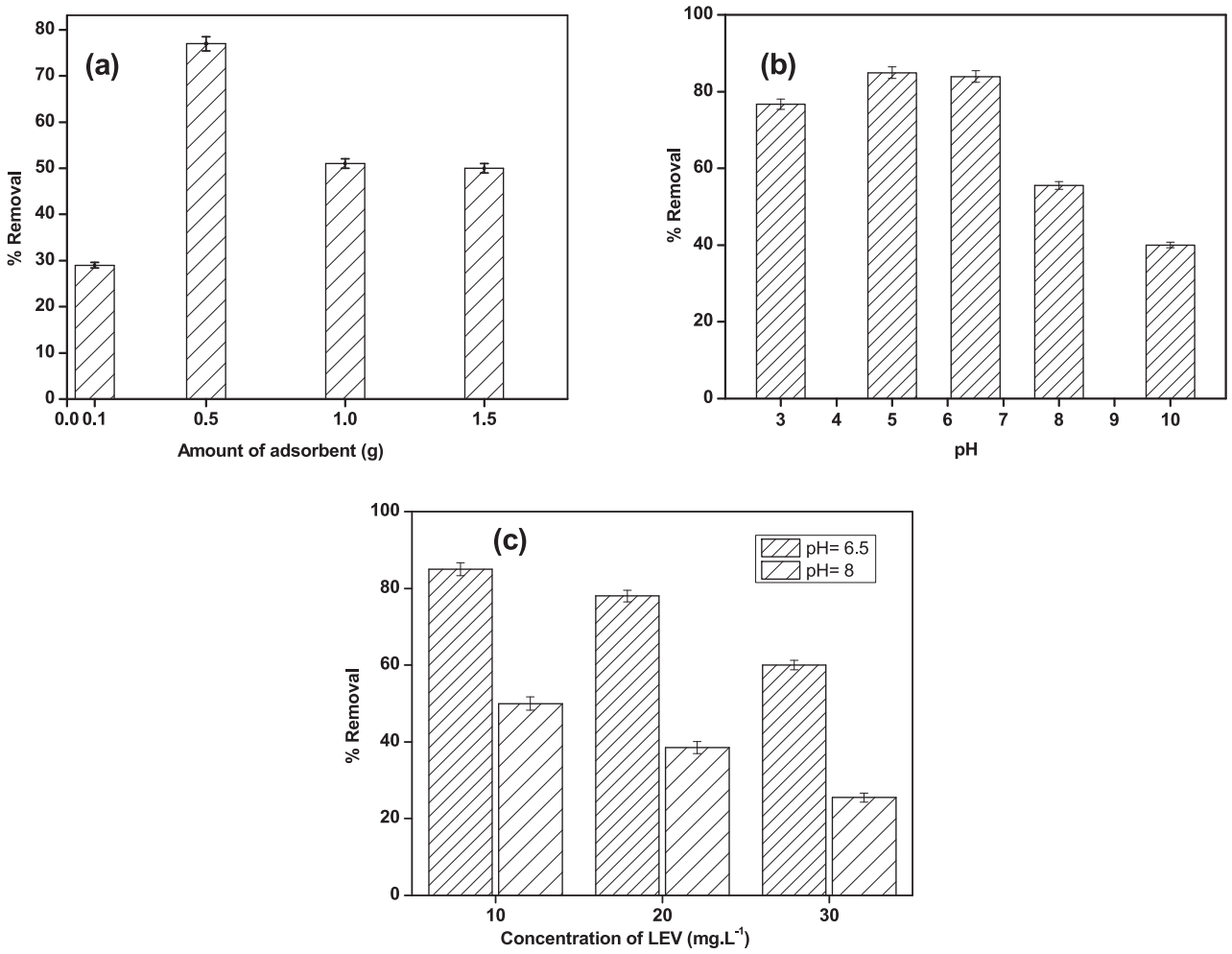

Fig. 6 Effect of (a) amount of adsorbent, (b) pH, and (c) initial adsorbate concentration on removal efficiency at 298 K.

contact time (min). The relationship was obtained by plotting $\ln(q_e - q_t)$ versus contact time. The values of k_1 and q_e were obtained from the slope and the axis intercept, respectively.

Another kinetic model, the linearized pseudo-second-order based on the Ho relation was investigated to fit the experimental data Eq.(4) (Ho, 2014; Benjelloun et al., 2021).

$$\frac{t}{Q} = \frac{1}{k_2 Q_e^2} + \frac{1}{Q_e} t \tag{4}$$

Where Q denotes the amount of LEV adsorbed on the adsorbent (mg/g). Q_e is the amount of LEV adsorbed on the adsorbent at equilibrium (mg/g). k_2 is the rate constant of pseudo-second-order adsorption g/(mg·min), and the contact time is denoted by t (min). Fig. 7 depicts the linear fits obtained using the pseudo-second-order kinetic model.

The Kinetic parameters extracted from Fig. 7 are listed in Table 1. The parameters show that the correlation coefficient of data (R^2 values) fits better at both pH levels for the pseudo-second-order model than for the pseudo-first-order model. Furthermore, at all concentrations, the amount of LEV removed at equilibrium is greater at pH 6.5 than at pH 8, and the rate of adsorption (k) decreased as LEV concentration increased for both pH values.

4.4. Adsorption isotherm

The sorption of LEV on the surface of PG-Fe^0 composite was quantified using Langmuir and Freundlich isotherm models. Langmuir describes the adsorption of a monolayer surface on a solid with specific sites that are strongly identical and is based on the kinetic principle (Hall et al., 1966). To fit the experimental data, the linear form of Langmuir adsorption isotherm was used as shown in Eq.(5).

$$\frac{C_e}{Q_e} = \frac{1}{Q_m K_L} + \frac{C_e}{Q_m} \tag{5}$$

C_e denotes the LEV solution's equilibrium concentration (mg/L). The maximum amount of LEV (mg) adsorbed per gram of adsorbents for complete monolayer coverage is defined as Q_m(mg/g). The Langmuir constant is denoted by the symbol K_L (L/mg).

The slope and intercept for the linear plot of $\frac{C_e}{Q_e}$ versus C_e, as shown in Fig. 8 (a), were used to calculate the adsorption parameters Q_m and K_L, respectively. The Freundlich isotherm is another commonly used adsorption model that implies multilayer adsorption and can be used for heterogeneous adsorbent surfaces with different sites of variable adsorption

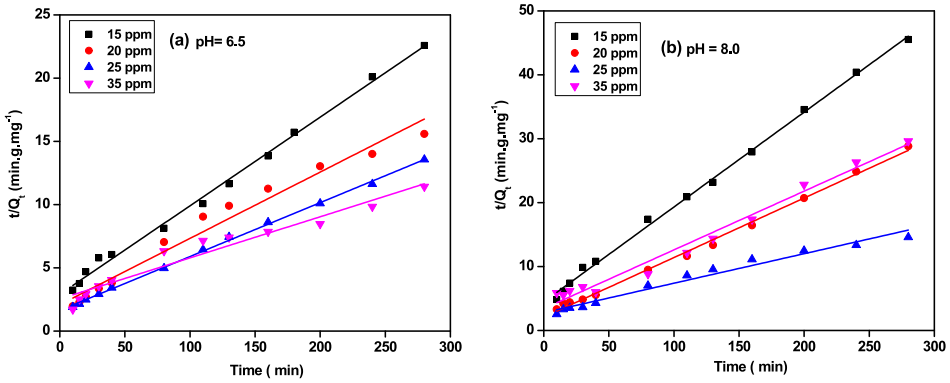

Fig. 7 Pseudo-second-order linear fits for the removal of LEV by PG-Fe^0 composite at (a) pH = 6.5 and (b) pH = 8, and 298 K.

Table 1 Kinetic parameters of LEV adsorption using PG-Fe0 composite at 298 K.

pH = 6.5		**Pseudo-first-order**			**Pseudo-second-order**		
C_0 **(mg/L)**	Q_e **(exp) (mg/g)**	R^2	$k_1\times10^3$**(min^{-1})**	Q_e **(cal) (mg/g)**	R^2	$k_2\times10^3$**g/(mg·min)**	Q_e **(cal) (mg/g)**
15	12.39	0.8279	10.9	7.806	0.9957	1.65	14.37
20	17.96	0.9399	9.40	13.52	0.9748	1.31	19.08
25	20.64	09,461	11.5	14.62	0.9970	1.22	23.15
30	24.51	0.8072	15.4	28.59	0.9512	0.41	30.76
pH = 8							
C_0 **(mg/L)**							
15	9.730	0.5920	13.6	4.721	0.9965	4.15	10.73
20	9.617	0.7596	12.8	9.602	0.9816	0.97	12.37
25	19.18	0.9635	9.60	16.81	0.9764	0.77	21.64
30	9.451	0.5073	10.3	3.894	0.9825	2.47	10.88

energy (Saadi et al., 2015). The linearized form of the Freundlich isotherm model is represented as:

$$lnQ_e = lnk_f + \left(\frac{1}{n}\right) lnC_e \tag{6}$$

The Freundlich constant (k_f) reflects the adsorption affinity and n is the Freundlich constant related to adsorption linearity. Both constants can be calculated from the slope and intercept of the linear plot of lnQ_e versus lnC_e, as shown in Fig. 8 (b). The parameters extracted from the Langmuir and Freundlich models at both pH values are shown in Table 2.

The R^2 values indicated that the experimental data at pH 6.5 was well fitted by both the Langmuir and Freundlich isotherm models. This data is consistent with the adapted LEV charge structure (zwitterionic), which allows for the formation of monolayer or multilayer adsorption between opposite ionic charges. At pH 8, the Langmuir isotherm model described the data better than the Freundlich isotherm, indicating monolayer adsorption between anionic LEV and composite. Furthermore, these results suggest a relation between the Freundlich model isotherm and the zwitterionic form of LEV which allows for multilayer adsorption.

The Q_m values confirmed these findings; the calculated maximum capacity of a composite at pH 6.5 is approximately 66.3 mg/g, while it is 11.4 mg/g at pH 8. These values are low when compared to the surface area of nano zero-valent iron adsorbents (131.3 m^2/g) (Al-Rimawi et al., 2022), but this is to be expected with bulky LEV molecules adsorbed in an aqueous solution versus physical adsorption of N_2 gas molecules on a solid surface. The LEV uptake capacity using PG-Fe^0 was compared to the capacities of other adsorbents reported in the literature (**Table S1**). The presented capacity demonstrated a moderate removal efficiency for LEV as toxic and biological active water pollutants; however, in terms of recovery, cost, and eco-friendly, the PG-Fe^0 composite still outperforms other adsorbents.

In the Freundlich model, the linearity of the adsorption or the degree of curvature for the isotherms over the concentration range is described by 1/n, which typically ranges from 1 to 0, and the value of 1/n less than 1 indicated a favorable adsorption process (Saadi et al., 2015).

4.5. Adsorption thermodynamic

The activation energy for LEV adsorption on the surface of PG-F^0 composite was calculated using the Arrhenius equation based on the kinetic data obtained at different temperatures, Eq.(7) (Logan, 1982).

$$ln\,k_2 = ln\,A - \frac{E_a}{RT} \tag{7}$$

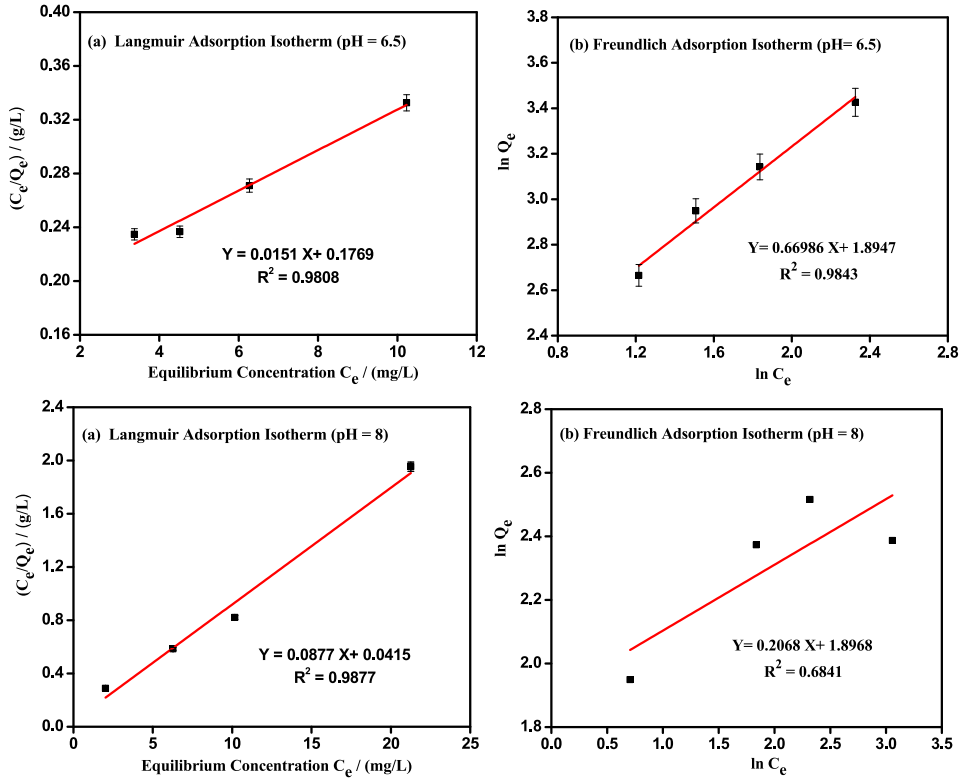

Fig. 8 Linear plots of (a) Langmuir isotherm model and (b) Freundlich isotherm model for LEV adsorption via PG- Fe^0 composite.

Table 2 Langmuir and Freundlich model parameters for LEV adsorption using a PG-Fe0 composite.

	Langmuir isotherm			Freundlich isotherm		
pH	R^2	Q_m	K_L	R^2	$1/n$	k_f
6.5	0.9808	66.3	0.09	0.9843	0.6686	6.657
8.0	0.9877	11.4	2.11	0.6841	0.2068	6.664

Where k_2 is the pseudo-second-order rate constant g/(mg·min), A is the pre-exponential factor, E_a is the activation energy (kJ/mol), R is the gas constant 8.314 J/(K·mol), and T is the absolute kelvin temperature (K). The slope for the linear plot of lnk_2 versus 1/T was used to calculate the value of E_a (Fig.S3). Other thermodynamic parameters were estimated including the heat of adsorption (standard enthalpy change, ΔH^o), standard entropy change (ΔS^o), and standard change in Gibbs free energy (ΔG^o). To evaluate the presented parameters, the thermodynamic Eqs. (8–9) were used.

The ΔH^o and ΔS^o values were determined using van't Hoff equation (Lima et al., 2020):

$$lnK_{eq} = \frac{\Delta S^{\circ}}{R} - \frac{\Delta H^{\circ}}{RT} \quad (8)$$

Where the K_{eq} is the equilibrium constant expressed as $\left(\frac{Q_e}{C_e}\right)$, and the value of ΔG^o was obtained from the following equations:

$$\Delta G^{\circ} = \Delta H^{\circ} - T\Delta S^{\circ} \quad (9)$$

The values of ΔH^o and ΔS^o were determined using the slope and y-axis intercept obtained from the linear plot of lnK_{eq} versus 1/T as shown in (Fig.S4), and the thermodynamic parameters were determined and listed in Table 3.

The nature of sorption (chemisorption or physisorption) could be determined by the value of E_a or from the value of ΔH^o. The magnitude of activation energy indicates whether the adsorption mechanism is physisorption (5 to 40 kJ/mol) or chemisorption (40 to 800 kJ/mol) (Abramian and El-Rassy, 2009). However, the negative activation energy makes a difficult decisive conclusion about the nature of adsorption (Atkins et al., 2014). Depending on the value of ΔH^o, the calculated value (44.4 kJ/mol) is in the range of chemisorption (> 40 kJ/mol) which was also confirmed by the FTIR analysis. Furthermore, the positive value of ΔH^o implies that the adsorption process is endothermic.

Previous research has led to the conclusion that a negative value for ΔG^o indicates that the adsorption process is spontaneous. In this study, the negative value of ΔG^o indicates that LEV is naturally adsorbed by the adsorbent at 288 K, and the

Table 3 Thermodynamic parameters of LEV adsorption at pH = 6.5.

pH	E_a(kJ/mol)	ΔH^o(kJ/mol)	ΔS^o(J/mol)	ΔG^o(kJ/mol)			
				278 K	288 K	298 K	308 K
6.5	−52.7	44.4	156.8	0.81	−0.76	−2.33	−3.89

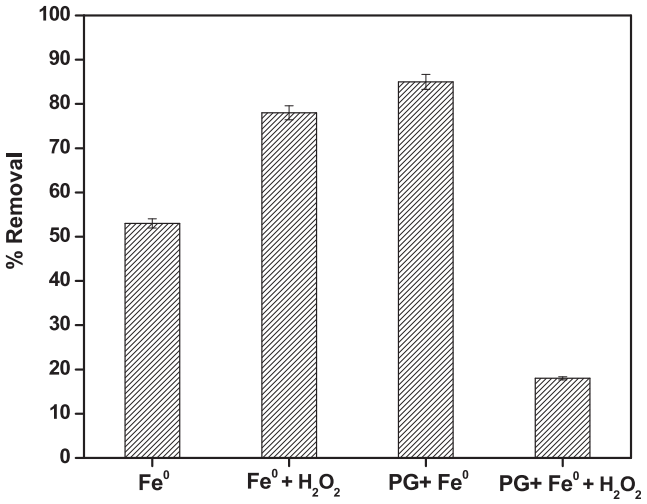

Fig. 9 Removal % of LEV using Fe^0 and PG-Fe^0 as adsorbents and as a Fenton-like catalyst.

value of ΔG^o decreases as the temperature increases, indicating that LEV adsorption is more favorable at high temperatures.

4.6. Removal of LEV by a Fenton-like process.

One of the most effective methods for degrading organic contaminants is the Fenton catalyst. The Fenton reagent can be generated by a cyclic process in an aqueous solution from the interaction of Fe^{2+} and H_2O_2. When ferrous ions are replaced by Fe^0 or iron oxides, a Fenton-like reaction occurs. The radicals are produced by reactions that occur during a Fenton-like cycle in which Fe^0 is used as a source of Fe^{2+} ions, and the radical can chemically oxidize and mineralize the organic pollutants (Neyens and Baeyens, 2003):

(i) $Fe^0 + 2H_2O_2 \rightarrow Fe^{2+} + 2\bullet OH + 2OH^-$
(ii) $Fe^{2+} + 2H_2O_2 \rightarrow Fe^0 + 2\bullet OOH + 2H^+$.

Fig. 9 depicts the results of related experiments, the results show that using PG-Fe^0 composite to eliminate the LEV has nearly the same removal efficiency as a Fenton-like reaction of ($Fe^0 + H_2O_2$) and is better than using bare Fe^0. On the other hand, Using PG-Fe^0 in presence of H_2O_2 reduced the

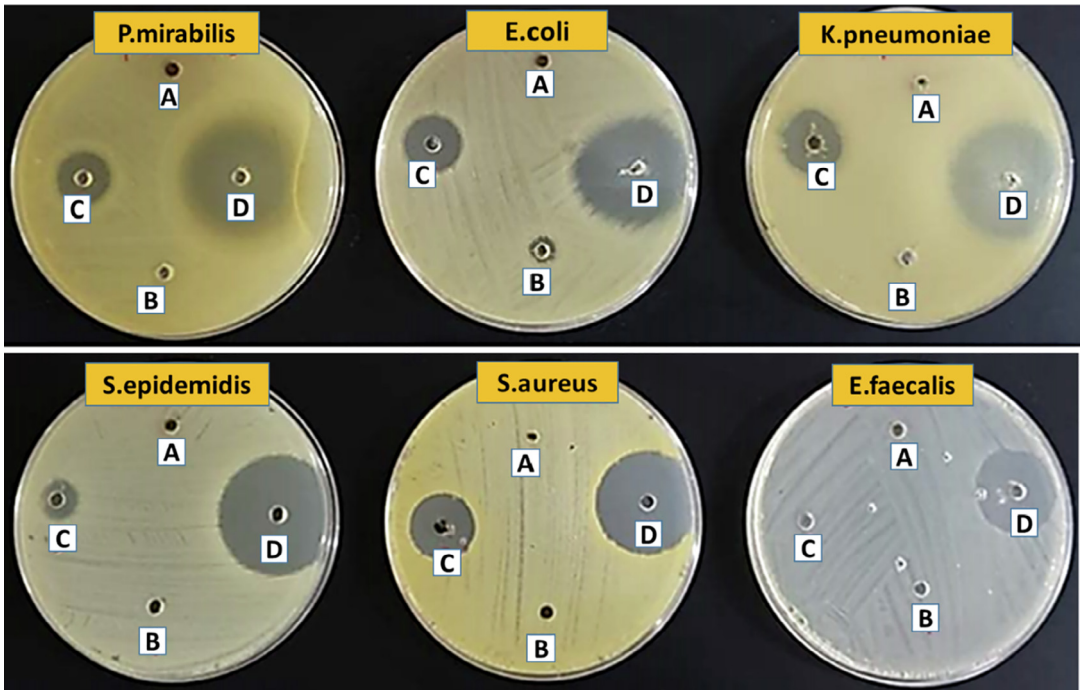

Fig. 10 Photographs of Petri plates used in the agar well diffusion method; (A) negative control (water), (B) PG-Fe^0, (C) PG-Fe^0-LEV, and (D) LEV, at pH = 6.5.

Table 4 Antibacterial activity of PG-Fe0, LEV, PG-Fe0-LEV, and negative control (water) in terms of zone inhibition via agar-well diffusion method at pH = 6.5.

Type of bacteria	Diameter of inhibition zone (mm)			
	PG-Fe^0 composite	Levofloxacin (LEV)	PG-Fe^0-LEV	Negative control (Water)
E.Coli	6.0	45.4	25.7	6.0
K.pneumoniae	6.0	45.9	28.8	6.0
P.mirabilis	6.0	40.7	24.1	6.0
S.epidemidis	6.0	46.2	15.1	6.0
S.aureus	6.0	44.1	21.8	6.0
E.faecalis	6.0	34.3	6.00	6.0

removal efficiency to 18 % under the same conditions. This behavior could be attributed to the LEV degradation cycle being hindered by the trapping of the radical produced during the Fenton-like process, or the adsorption of LEV molecules on the surface of Fe^0 prevents the formation of radical, additionally, the Fenton-like process is very sensitive to pH value (Zhang, 2003; Poursaberi et al., 2012; Nazari et al., 2013). However, when the removal efficiency of PG-Fe^0 is compared to that of the Fenton-like reaction, the proceeding method using PG-Fe^0 as an adsorbent significantly outperforms the Fenton-like performance because the Fenton-like process produces a lot of more toxic degraded substances that harm the environment than the parent compound.

4.7. Antibacterial activity

The future of PG-Fe^0 composite can be used to reduce environmental pollution and control the release of antibiotics in drug delivery systems. Therefore, there is a great opportunity for the recovery, reusability, and recycling of a large number of antibiotics using the synthesized PG-Fe^0 composite.

The reusability of the adsorbed LEV and the antibacterial activity of PG-Fe^0-LEV composite against various bacterial strains was investigated. The lack of growth of bacteria or microorganisms is observed in the area around the hole known as the inhibition zone, and the effectiveness of the LEV antibiotic increases at a specific concentration on various types of bacterial strains. Fig. 10 depicts the antibacterial activity of PG-Fe^0 composite, LEV, PG-Fe^0-LEV, and water (negative control) in terms of zone inhibition as measured by the agar well diffusion method at pH 6.5. The antibacterial activity was investigated by comparing the effectiveness of pure LEV and PG-Fe^0-LEV for inhibiting the effect of the bacterial strain. The calculated suppression zone diameter is shown in Table 4, in all tested samples, no antibacterial activity was detected for the PG-Fe^0 composite. The antibacterial activity of PG-Fe^0-LEV on the bacterial strains was irregular and did not show a significant effect on the Enterococcus faecalis strain. In addition, the results show that the LEV activity after adsorption on the surface of the PG-Fe^0 composite varies from that of the pure LEV drug. Despite the PG-Fe^0-LEV composite having a lower effect than pure LEV, the new combination between the active LEV molecules and the PG-Fe^0 composite does not destroy LEV's bacterial inhibition mechanism as an antibiotic. Furthermore, the biological activity test shows the possible influence of LEV on bacterial life in the aquatic environment.

5. Conclusions

The chemical structure of LEV is pH-dependent, and the pH value influences LEV's maximum removal efficiency. PG-Fe^0 composite was prepared and used as an efficient adsorbent for the removal of LEV from an aqueous solution. The synthesized composite and adsorption process were characterized and analyzed using various techniques. The kinetic and thermodynamic parameters were investigated at different pH values, adsorbent dose, initial LEV concentration, and contact time. The adsorption data fitted the pseudo-second-order model at both pH values (6.5 and 8). The Langmuir isotherm model is valid at pH 8, while the Freundlich isotherm is applicable at both pH values. In addition, the thermodynamic parameters indicated an endothermic chemisorption process, and the LEV adsorption is favorable at high temperatures. Furthermore, the PG-Fe^0 composite was examined and compared as a catalyst in a Fenton-like reaction. The reusability and antimicrobial activity of the adsorbed LEV molecules (PG-Fe^0-LEV) were tested against various types of bacterial strains, the results indicated that the LEV may have an impact on bacterial life in the aquatic environment. Finally, the PG-Fe^0 composite has shown an ability to reduce pollutants and potentially control antibiotic reuse.

Declaration of Competing Interest

The authors declare that they have no known competing financial interests or personal relationships that could have appeared to influence the work reported in this paper.

Acknowledgment

The authors would like to thank the financial support received from the Scientific Research Committee at Birzeit University. The authors would also like to thank their colleagues from Birzeit University: A.N. Dudin, and I. Shalash for their technical support.

Appendix A. Supplementary data

Supplementary data to this article can be found online at https://doi.org/10.1016/j.arabjc.2022.104309.

References

Abramian, L., El-Rassy, H., 2009. Adsorption kinetics and thermodynamics of azo-dye Orange II onto highly porous titania aerogel. Chem. Eng. J. 150, 403–410.

Agrawal, B., 2008. Engineering Drawing. Tata McGraw-Hill Education.

Alabdali, A.J., Ibrahim, F.M., 2014. Synthesis and Thermal Study of Co (II), Ni (II), Cu (II) Mixed Ligand Complexes Using Histidine As Tridentate Ligand. IOSR J. Appl. Chem. (IOSR-JAC) 6, 60–63.

Al-Jabari, M.H., Sulaiman, S., Ali, S., et al, 2019. Adsorption study of levofloxacin on reusable magnetic nanoparticles: Kinetics and antibacterial activity. J. Mol. Liq. 291, 111249.

Al-Rimawi, L.N., Al-Jabari, M.H., Sulaiman, S.M., et al, 2022. Pencil graphite synergistic improvement of zero-valent iron composite for the removal of diclofenac sodium in aqueous solutions: Kinetics and comparative study. Adv. Powder Technol. 33, 103610.

Anderson, V.R., Perry, C.M., 2008. Levofloxacin. Drugs. 68, 535–565.

Ashfaq, M., Khan, K.N., Rasool, S., et al, 2016. Occurrence and ecological risk assessment of fluoroquinolone antibiotics in hospital waste of Lahore. Pakistan. Environmental toxicology and pharmacology. 42, 16–22.

Atkins, P., Atkins, P.W., de Paula, J., 2014. Atkins' physical chemistry. Oxford University Press.

Ben Arfi, R., Karoui, S., Mougin, K., et al, 2017. Adsorptive removal of cationic and anionic dyes from aqueous solution by utilizing almond shell as bioadsorbent. Euro-mediterranean journal for environmental integration. 2, 1–13.

Benjelloun, M., Miyah, Y., Evrendilek, G.A., et al, 2021. Recent advances in adsorption kinetic models: their application to dye types. Arabian J. Chem. 14, 103031.

Chen, Z.-X., Jin, X.-Y., Chen, Z., et al, 2011. Removal of methyl orange from aqueous solution using bentonite-supported nanoscale zero-valent iron. J. Colloid Interface Sci. 363, 601–607.

David, I.G., Popa, D.-E., Buleandra, M., 2017. Pencil graphite electrodes: a versatile tool in electroanalysis. J. Anal Methods Chem., 2017

Fu, C., Zhu, X., Dong, X., et al, 2021. Study of adsorption property and mechanism of lead (II) and cadmium (II) onto sulfhydryl modified attapulgite. Arabian J. Chem. 14, 102960.

Gong, Y., Wang, Y., Lin, N., et al, 2022. Iron-based materials for simultaneous removal of heavy metal (loid) s and emerging organic contaminants from the aquatic environment: Recent advances and perspectives. Environ. Pollut. 118871.

Graham, D.W., deNoyelles, F.J., Lydy, M.J., et al, 2006. Fate and Effects of Fluoroquinolone Antibacterial Agents in Aquatic Ecosystems. University of Kansas, USA.

Hall, K.R., Eagleton, L.C., Acrivos, A., et al, 1966. Pore-and solid-diffusion kinetics in fixed-bed adsorption under constant-pattern conditions. Ind. Eng. Chem. Fundam. 5, 212–223.

Ho, Y.-S., 2014. Using of "pseudo-second-order model" in adsorption. Environ. Sci. Pollut. Res. 21, 7234–7235.

Ji, Y.-X., Wang, F.-H., Duan, L.-C., et al, 2013. Effect of temperature on the adsorption of sulfanilamide onto aluminum oxide and its molecular dynamics simulations. Appl. Surf. Sci. 285, 403–408.

Kemper, N., 2008. Veterinary antibiotics in the aquatic and terrestrial environment. Ecol. Ind. 8, 1–13.

Kolahi-Ahari, S., Deiminiat, B., Rounaghi, G.H., 2020. Modification of a pencil graphite electrode with multiwalled carbon nanotubes capped gold nanoparticles for electrochemical determination of tramadol. J. Electroanal. Chem. 862, 113996.

Li, X.-Q., Elliott, D.W., Zhang, W.-X., 2008. Zero-valent iron nanoparticles for abatement of environmental pollutants: materials and engineering aspects. Particulate Systems in Nano-and Biotechnologies, CRC Press, 309–330.

Lima, E.C., Gomes, A.A., Tran, H.N., 2020. Comparison of the nonlinear and linear forms of the van't Hoff equation for calculation of adsorption thermodynamic parameters (Δ S° andΔ H°). J. Mol. Liq. 311, 113315.

Liu, N., Fei, F., Dai, W., et al, 2022. Visible-light-assisted persulfate activation by SnS2/MIL-88B (Fe) Z-scheme heterojunction for enhanced degradation of ibuprofen. J. Colloid Interface Sci. 625, 965–977.

Logan, S., 1982. The origin and status of the Arrhenius equation. J. Chem. Educ. 59, 279.

Luo, Y., Guo, W., Ngo, H.H., et al, 2014. A review on the occurrence of micropollutants in the aquatic environment and their fate and removal during wastewater treatment. Sci. Total Environ. 473, 619–641.

Mimouni, F.Z., Belboukhari, N., Sekkoum, K., et al, 2018. A Comparison between Experimental and Theoretical Spectroscopic Data of Ofloxacin. Der Pharma Chemica. 10, 31–35.

Nazari, S., Yari, A.R., Mahmodian, M.H., et al., 2013. Application of H2O2 and H2O2/Fe0 in removal of Acid Red 18 dye from aqueous solutions.

Neyens, E., Baeyens, J., 2003. A review of classic Fenton's peroxidation as an advanced oxidation technique. J. Hazard. Mater. 98, 33–50.

Park, H.-R., Kim, T.H., Bark, K.-M., 2002. Physicochemical properties of quinolone antibiotics in various environments. Eur. J. Med. Chem. 37, 443–460.

Ponder, S.M., Darab, J.G., Mallouk, T.E., 2000. Remediation of Cr (VI) and Pb (II) aqueous solutions using supported, nanoscale zero-valent iron. Environ. Sci. Technol. 34, 2564–2569.

Poursaberi, T., Hassanisadi, M., Nourmohammadian, F., 2012. Application of synthesized nanoscale zero-valent iron in the treatment of dye solution containing basic yellow 28.

Qassim, A.W., 2015. Determination of Levofloxacin in pharmaceutical formulation tavanic by Visible spectrophotometry of its chelating complex with aluminum ion (iii). Int. J. Dev. Res. 5, 4702–4706.

Qian, L., Liu, S., Zhang, W., et al, 2019. Enhanced reduction and adsorption of hexavalent chromium by palladium and silicon rich biochar supported nanoscale zero-valent iron. J. Colloid Interface Sci. 533, 428–436.

Qin, X., Liu, F., Wang, G., et al, 2014. Adsorption of levofloxacin onto goethite: effects of pH, calcium and phosphate. Colloids Surf., B 116, 591–596.

Saadi, R., Saadi, Z., Fazaeli, R., et al, 2015. Monolayer and multilayer adsorption isotherm models for sorption from aqueous media. Korean J. Chem. Eng. 32, 787–799.

Samuelsen, O.B., 2006. Pharmacokinetics of quinolones in fish: a review. Aquaculture 255, 55–75.

Schlüsener, M.P., Bester, K., 2006. Persistence of antibiotics such as macrolides, tiamulin and salinomycin in soil. Environ. Pollut. 143, 565–571.

Shen, G., Pan, L., Zhang, R., et al, 2020. Low-spin-state hematite with superior adsorption of anionic contaminations for water purification. Adv. Mater. 32, 1905988.

Simonin, J.-P., 2016. On the comparison of pseudo-first order and pseudo-second order rate laws in the modeling of adsorption kinetics. Chem. Eng. J. 300, 254–263.

Skrzypczynska, K., Kusmierek, K., Swiatkowski, A., et al, 2018. The influence of pencil graphite hardness on voltammetric detection of pentachlorophenol. Int. J. Electrochem. Sci. 13, 88–100.

Sulaiman, S.M., Al-Jabari, M.H., 2021. Enhanced adsorptive removal of diclofenac sodium from aqueous solution by bentonite-supported nanoscale zero-valent iron. Arab Journal of Basic and Applied Sciences. 28, 51–63.

Sulaiman, S., Shahwan, T., 2017. Mefenamic acid stability and removal from wastewater using bentonite-supported nanoscale zero-valent iron and activated charcoal. Desalin. Water Treat. 97, 175–183.

Sun, Y.-P., Li, X.-Q., Cao, J., et al, 2006. Characterization of zero-valent iron nanoparticles. Adv. Colloid Interface Sci. 120, 47–56.

Tavares, P.H.C.P., Barbeira, P.J.S., 2008. Influence of pencil lead hardness on voltammetric response of graphite reinforcement carbon electrodes. J. Appl. Electrochem. 38, 827–832.

Taylor, A., 2013. Design essentials for the motion Media artist: A practical guide to principles & techniques. Routledge.

Thilagan, J., Gopalakrishnan, S., Kannadasan, T., 2013. A comparative study on adsorption of copper (ii) ions in aqueous solution by; (a) chitosan blended with cellulose and cross linked by formaldehyde,(b) chitosan immobilised on red soil,(c) chitosan reinforced by banana stem fibre. Int. J. Appl. Eng. Technol. 3, 35–60.

Turel, I., 2002. The interactions of metal ions with quinolone antibacterial agents. Coord. Chem. Rev. 232, 27–47.
Uivarosi, V., 2013. Metal complexes of quinolone antibiotics and their applications: an update. Molecules 18, 11153–11197.
Verlicchi, P., Galletti, A., Petrovic, M., et al, 2010. Hospital effluents as a source of emerging pollutants: an overview of micropollutants and sustainable treatment options. J. Hydrol. 389, 416–428.
Vijayakumar, G., Tamilarasan, R., Dharmendirakumar, M., 2012. Adsorption, Kinetic, Equilibrium and Thermodynamic studies on the removal of basic dye Rhodamine-B from aqueous solution by the use of natural adsorbent perlite. J. Mater. Environ. Sci. 3, 157–170.
Wang, Y., Gong, Y., Lin, N., et al, 2022a. Cellulose hydrogel coated nanometer zero-valent iron intercalated montmorillonite (CH-MMT-nFe0) for enhanced reductive removal of Cr (VI): Characterization, performance, and mechanisms. J. Mol. Liq. 347, 118355.
Wang, Y., Gong, Y., Lin, N., et al, 2022b. Enhanced removal of Cr (VI) from aqueous solution by stabilized nanoscale zero valent iron and copper bimetal intercalated montmorillonite. J. Colloid Interface Sci. 606, 941–952.
Wang, N., Wang, Y.-F., Omer, A.M., et al, 2017. Fabrication of novel surface-imprinted magnetic graphene oxide-grafted cellulose nanocrystals for selective extraction and fast adsorption of fluoroquinolones from water. Anal. Bioanal. Chem. 409, 6643–6653.
Wang, Y., Wang, Y., Yu, L., et al, 2020. Highly effective microwave-induced catalytic degradation of Bisphenol A in aqueous solution using double-perovskite intercalated montmorillonite nanocomposite. Chem. Eng. J. 390, 124550.
Xu, C., Yang, W., Liu, W., et al, 2018. Performance and mechanism of Cr (VI) removal by zero-valent iron loaded onto expanded graphite. J. Environ. Sci. 67, 14–22.
Yang, Y., Gu, Y., Lin, H., et al, 2022a. Bicarbonate-enhanced iron-based Prussian blue analogs catalyze the Fenton-like degradation of p-nitrophenol. J. Colloid Interface Sci. 608, 2884–2895.
Yang, Y., Li, X., Jie, B., et al, 2022b. Electron structure modulation and bicarbonate surrounding enhance Fenton-like reactions performance of Co-Co PBA. J. Hazard. Mater. 437, 129372.
Yu, C., Shao, J., Sun, W., et al, 2020. Treatment of lead contaminated water using synthesized nano-iron supported with bentonite/graphene oxide. Arabian J. Chem. 13, 3474–3483.
Yuan, P., Annabi-Bergaya, F., Tao, Q., et al, 2008. A combined study by XRD, FTIR, TG and HRTEM on the structure of delaminated Fe-intercalated/pillared clay. J. Colloid Interface Sci. 324, 142–149.
Zhang, W.-X., 2003. Nanoscale iron particles for environmental remediation: an overview. J. Nanopart. Res. 5, 323–332.
Zhu, Z., Rao, R., Zhao, Z., et al, 2022. Research progress on removal of phthalates pollutants from environment. J. Mol. Liq. 118930.